J Neurophysiol 101: 3226–3234, 2009.
First published April 8, 2009; doi:10.1152/jn.91349.2008.

Spike-Timing–Dependent Synaptic Plasticity and Synaptic Democracy in Dendrites

Albert Gidon[1] and Idan Segev[1,2]
[1]*Department of Neurobiology and* [2]*Interdisciplinary Center for Neural Computation, The Hebrew University, Jerusalem, Israel*

Submitted 22 December 2008; accepted in final form 6 April 2009

Gidon A, Segev I. Spike-timing–dependent synaptic plasticity and synaptic democracy in dendrites. *J Neurophysiol* 101: 3226–3234, 2009. First published April 8, 2009; doi:10.1152/jn.91349.2008. We explored in a computational study the effect of dendrites on excitatory synapses undergoing spike-timing–dependent plasticity (STDP), using both cylindrical dendritic models and reconstructed dendritic trees. We show that even if the initial strength, g_{peak}, of distal synapses is augmented in a location independent manner, the efficacy of distal synapses diminishes following STDP and proximal synapses would eventually dominate. Indeed, proximal synapses always win over distal synapses following linear STDP rule, independent of the initial synaptic strength distribution in the dendritic tree. This effect is more pronounced as the dendritic cable length increases but it does not depend on the dendritic branching structure. Adding a small multiplicative component to the linear STDP rule, whereby already strong synapses tend to be less potentiated than depressed (and vice versa for weak synapses) did partially "save" distal synapses from "dying out." Another successful strategy for balancing the efficacy of distal and proximal synapses following STDP is to increase the upper bound for the synaptic conductance (g_{max}) with distance from the soma. We conclude by discussing an experiment for assessing which of these possible strategies might actually operate in dendrites.

INTRODUCTION

Donald O. Hebb (1949) introduced his famous postulate for the mechanism that may underlie activity-dependent synaptic plasticity 60 years ago. In the last 10 years, experimental studies have begun to unravel the operation of such a mechanism and it has been shown that, in many neuron types, the precise timing of the pre-versus the postsynaptic spikes play a critical role in determining the efficacy of the synaptic connection between neurons [spike-timing–dependent plasticity (STDP)] (Bell et al. 1997; Bi and Poo 1998; Debanne et al. 1998; Markram et al. 1997; Zhang et al. 1998; reviews by Dan and Poo 2006 and Abbott and Nelson 2000). This specific type of synaptic plasticity operates within a time window of tens of milliseconds, and its direction and magnitude are critically determined by the temporal order of the pre- versus the postsynaptic spike. If a synapse is active before the postsynaptic neuron fired a spike (pre before post), the efficacy of this synapse is enhanced; the synapse is weakened for the reverse temporal order (post before pre). Outside of the critical temporal window for STDP, the efficacy of the synapse remains unchanged.

These experimental studies were followed by theoretical efforts to understand the biophysical foundation of STDP (Shouval et al. 2002), as well as its possible functional consequences (Gütig et al. 2003; Kempter et al. 2001; Kistler and van Hemmen 2000; Roberts 2000; Roberts and Bell 2000; Rubin 2001; Rubin et al. 2001; Song and Abbott 2001; Song et al. 2000; van Rossum et al. 2000; Williams et al. 2003 and see a whole issue of *Biological Cybernetics* in December 2002 dedicated to STDP). Among the possible functional roles attributed to STDP are the emergence of functional maps during development (Song and Abbott 2001), enhancement of correlated inputs (Gütig et al. 2003; Meffin et al. 2006; van Rossum et al. 2000), enhancement of input temporal precision (Kistler and van Hemmen 2000), and the generation of a negative sensory image (Roberts and Bell 2000).

One interesting question regarding STDP is its role in selectively "configuring" the synaptic efficacy at different dendritic locations. Because neurons are inhomogeneous in their morphology and membrane properties, synaptic contacts at different locations on the dendrite would be influenced by different specific dendritic attributes such as calcium concentrations or the back propagating action potential (BPAP), and this may affect synaptic efficacy in dendrites differentially (Iannella and Tanaka 2006; Rao and Sejnowski 2001; Saudargiene et al. 2005a,b; Urakubo et al. 2004; and see also Rabinowitch and Segev 2006). Indeed, several recent experimental studies have beautifully shown the regional specificity of STDP in dendrites (Froemke et al. 2005; Letzkus et al. 2006; Sjöström and Häusser 2006). This interaction between STDP and dendrites is the focus of this computational study. We first show that there is an inherent problem when applying the linear STDP rule in dendrites with excitatory synapses. We show that this rule is "anti-democratic" in nature so that applying it to dendritic synapses would result in the complete degradation of the efficacy of distal excitatory synapses and would maximally elevate the efficacy of proximal synapses (Rumsey and Abbott 2004, 2006). In this case, a simple upscaling of the peak conductance of distal synapses does not solve this problem. In our study, we systematically explore the dendritic attributes such as length and branching and their relation to this problem. Finally, we discuss a possible robust mechanism that enable the co-existence of proximal and distal synapses undergoing STDP and propose an experimental prediction to whether it actually operates in dendrites.

METHODS

Compartmental models

In most of the simulations, the neuron model consisted of a passive cylindrical cable connected to an isopotantial soma. Unless otherwise stated, the cylinder was one space constant (λ) long with 50 compartments per λ. In Fig. 3, we simulated a set of idealized dendritic trees (from 0th to 3rd order of branching) that are equivalent to a single

Address for correspondence: A. Gidon, The Hebrew Univ., Edmond J. Safra Campus, Givat Ram Jerusalem 91904, Israel (E-mail: agidon20@lobster.ls.huji.ac.il).

cylindrical cable (Rall 1959). In Fig. 4, we implemented the STDP rule to models of reconstructed neurons; L4 spiny stellate cell (Ascoli 2006; Vetter et al. 2001) L2/3 pyramidal cell (Ascoli 2006; Vetter et al. 2001), and L5 pyramid (Douglas et al. 1991). The specific membrane capacitance of all models used was $C_m = 1\ \mu F/cm^2$; the axial resistance $R_a = 100\ \Omega cm$, and the passive membrane resistance $R_m = 20{,}000\ \Omega cm^2$ (the membrane time constant, τ_m, is 20 ms). Resting potential was set at −70 mV. The soma was identical in all of the models (area $5 \times 10^{-5}\ cm^2$—including the idealized and reconstructed neurons). Dendritic spines were not included in the models.

Firing mechanism

In addition to $g_{leak} = 1/R_m$, the modeled soma also included fast inactivating sodium currents, I_{Na}, and potassium delayed rectifier I_{Kdr} currents, with the following specific maximal conductances and corresponding reversal potentials: $g_{Na} = 0.03\ S/cm^2$; $g_K = 0.015\ S/cm^2$; $E_K = -80$ mV; $E_{Na} = 90$ mV. The rate functions for the sodium and potassium channels where taken from Traub et al. (1991), with a slight modification for the potassium channels whereby the activation time constant, τ_n, was reduced by a factor of 2.

Synaptic input

Transient excitatory synaptic conductance change was modeled by a single decaying exponent (ExpSyn in NEURON) with a time constant of 5 ms and a reversal potential of 0 mV. The activation time of the synapse was drawn from a random Poisson process with identical mean interval for all synapses.

The weight (strength) of the ith synapses, w_i, is defined as $w_i = g_{peak,i}/g_{max,i}$, where $g_{peak,i}$ is the peak conductance of the ith synapse, which ranges between 0 and $g_{max,i}$ (the notation i is mostly omitted). g_{max} was uniformly set to 0.3 nS in all figures except in Figs. 6. Note that w must be treated with caution when comparing synapses that have different g_{max} values, because in this case, synapses with identical w would have different peak conductances.

Each compartment in the cylinder consisted of 16 conductance-based excitatory synapses, yielding a total of 800 synapses per λ. In Fig. 3*B*, a total of 960 synapses were distributed with a fixed density per unit area, so that the number of synapses in any given electrotonic distance from the soma is identical regardless of the branching order. In Fig. 3*C*, synapses where distributed at a density of 600 per λ. Consequently, a zeroth-order (cylinder) tree contained 600 synapses, whereas the dendrite of a third-order tree contained 2,250 synapses.

For all reconstructed trees (Fig. 4), the synaptic density was uniformly set to $0.02/\mu m^2$. This yielded a total of 283, 378, and 1,060 synapses for the L4, L2/3, and L5 cells, respectively.

Modeling different STDP rules

When using an additive (or linear) STDP rule, synaptic plasticity is updated according to the temporal difference between the pre- and the post-synaptic spikes

$$\Delta w_+ = A_+ \exp(-(t_{post} - t_{pre})/\tau) \text{ if } t_{post} \geq t_{pre} \quad (1)$$

$$\Delta w_- = A_- \exp(-(t_{post} - t_{pre})/\tau) \text{ if } t_{post} < t_{pre} \quad (2)$$

where $\Delta w_\pm$ is an increment/decrement in w in each update.

The amplitude of the synaptic modification is determined by the value of A_+ for potentiation and by A_- for depression. A_+ and A_- were set to 0.01 and −0.0105, respectively, and $\tau = 20$ ms as in Song et al. (2000).

Unless otherwise mentioned, the additive STDP rule was used. We also used another variation of the STDP rule—the multiplicative STDP rule (Gütig et al. 2003). In the multiplicative case, a term that involves the dependence of STDP on the value of synaptic weights was added to *Eqs. 1* and *2* above

$$\Delta w_+ = (1 - w)^\mu \times A_+ \exp(-(t_{post} - t_{pre})/\tau) \text{ if } t_{post} \geq t_{pre} \quad (3)$$

$$\Delta w_- = w^\mu \times A_- \exp(-(t_{post} - t_{pre})/\tau) \text{ if } t_{post} < t_{pre} \quad (4)$$

In this case, the degree of potentiation of already strong synapses is smaller than the degree of their depression and vice versa for weak synapses. The power μ determines the degree of dependence of the plasticity on the current synaptic weights; μ ranges between 0 (additive) and 1 (fully multiplicative).

In this study, we implemented the STDP rule in the "all to all" interaction, whereby all the possible combinations of pairing between the pre- and the postsynaptic spikes are linearly summed. For a given postsynaptic spike, all the synapses that fire before the spike are potentiated (to a degree which depends on their time difference, $t_{post} - t_{pre}$), whereas all the synapses firing after the spike are depressed (see also Bi and Wang 2002; Froemke and Dan 2002; Froemke et al. 2006; Sjöström et al. 2001).

In Figs. 1 and 6, synapses having equal efficacies as measured at the soma were obtained by initially implementing an anti-STDP rule as in Rumsey and Abbott (2004). In this case, whenever a synapse is activated, its weight is increased by a constant value (here we used $K_{Rumsey} = 0.0048$), whereas if the synapse generates a spike, it is weakened according to the anti-STDP rule.

Activity-dependent length constant of dendrites

In Fig. 6, we used a measure for the activity-dependent λ. Because the effective membrane conductance also depends on the synaptic conductances that impinges on the dendrite, λ changes with time and modification of synaptic weights during STDP. λ_{eff} is therefore measured in steady state

$$\lambda_{eff} = \frac{1}{t^* l} \int_0^l \int_0^{t^*} \lambda(x, t) \mathrm{d}t \mathrm{d}x \quad (5)$$

where t^* is a time interval, l is the physical length of the dendritic cylinder, and $\lambda(x,t)$ is

$$\lambda(x, t) = \sqrt{\frac{d}{4R_a}} \times \sqrt{\frac{1}{G_m(x, t)}} \quad (6)$$

where d is the cylinder's diameter and G_m (specific membrane conductance) comprises of the leak conductance in parallel with the synaptic conductances that vary with time and location in the dendrite. To compute λ_{eff} from the simulations, we used the discreet form of *Eq. 5*

$$\lambda_{eff} = \frac{1}{JK} \sum_{k=1}^{K} \sum_{j=1}^{J} \lambda_{kj} \quad (7)$$

where K is the number of compartments, and J is the number of discrete time steps. Combining *Eqs. 6* and *7*, we get

$$\lambda_{eff} = \frac{\sqrt{dl/(4R_a)}}{JK} \sum_{k=1}^{K} \sum_{j=1}^{J} \frac{1}{\sqrt{G_{kj}}} \quad (8)$$

Here, G_{kj} is the total membrane conductance in compartment k in time step j. This expression was evaluated every time step until the value of λ_{eff} converged.

β measure for the balance of the spatial distribution of synaptic weights

We propose a new measure, β, to describe the degree of balance in the spatial distribution of the synaptic weights

$$\beta = \frac{1}{NLW}\sum_{i=1}^{N} X_i w_i \quad (9)$$

where X_i is the electrotonic distance of the ith synapse, w_i is the weight of this synapse, L is the cable length of the cylindrical dendrite, W is the mean synaptic weight, and N the total number of synapses. Thus β is the location of the center of mass of the synaptic weights. When the synaptic weights are homogeneously distributed over the cylinder, then $\beta = 0.5$ (the center of mass is at the center of the cylinder). When the synaptic weights tend to be concentrated at one end of the cylinder, then β will approach either 0 (if all weights are concentrated near the proximal/soma end) or 1 (if all weights are concentrated near the distal end).

In all figures, β is plotted against W at steady state. To explore the dependence of β on W, we varied the final value of W by changing the input firing rate. As Song et al. (2000) showed, when the input rate is low, more synapses become strong, causing W to increase. In contrast, when the input rate is high, W typically tends to become small. In both cases (low or high input rate) where synapses are pushed to their extreme values (1 or 0, respectively), weight distribution is more balanced than for intermediate input rates. This gives us a characteristic convex β function as it appears in all the plots.

In Figs. 2*D* and 6*C*, β is plotted only for low values of W (<0.5) in some of the cases. The reason is that, for these cases, reaching a steady state with low input rates takes a very long time. We therefore set the lowest input rate to be 4 Hz (rightmost symbol in all cases), and the simulation ran until steady state is reached in all cases.

In Fig. 3*C* (branched dendrite), synapses are uniformly distributed per unit of length, hence their number increases with each additional branching point. Consequently, the weights distribution is not balanced to begin with because there are more synapses and hence more weights distally. To overcome this, we normalize the synaptic weight by number of synapses with the same distance.

Computing

All the simulations were performed under NEURON environment (Hines and Carnevale 1997) version 5.8 (or newer) with HOC and MOD programming languages. The computing resources included 32-bit Intel and 64-bit AMD computers. A backward Euler integration method (NEURON default) was used with a fixed integration time step of 0.1 ms. A typical run time of a simulation with 800 synapses until synaptic strength reaches steady-state values under STDP ranges between 4 hours for isopotential neurons and 4–5 days for the reconstructed neuron models. Simulation time was always $\geq 5 \times 10^4$ s. Steady state was determined after a reasonable amount of time where the synaptic distribution did not change significantly.

RESULTS

Problem with STDP and dendritic synapses

Figure 1 depicts the imbalanced distribution of the value of w at steady state that arises because of STDP (Goldberg et al. 2002; Roth and London 2004). Initially, identical synapses ($w = 0.5$, horizontal line in Fig. 1*C*) were distributed over a passive cylindrical dendrite. However, at steady state, distal synapses "died out" (weights were reduced to ~0), whereas proximal synapses tended to become maximally strong (Fig. 1*A*). The result is a bimodal distribution of the synaptic weights at steady state (Fig. 1*B*). This is the consequence of the passive dendritic filtering whereby the efficacy of synapses at the soma corresponds to their distance from the soma (Rall 1967). For initially identical synapses, the somatic excitatory postsynaptic potential (EPSP) that originates from a proximal synapse has larger amplitude than the one originating from a distal synapse. The competition caused by STDP drives strong (proximal) synapses to become even stronger, whereas weaker (distal) synapses eventually die out. Hence, in the passive case, the distribution of synaptic weights is bimodal (Fig. 1*B*) and the identity of the synapses that tend to win the competition is known in advance; the proximal synapses will always "beat" the distal synapses.

At steady state, the winning of the proximal synapses over the distal synapses takes place even in the extreme case whereby initially $w = 0$ for all proximal synapses and $w = 1$ for all distal synapses (Fig. 1*C*, gray lines).

Indeed, during the implementation of the STDP rule, even a weightless synapse may occasionally strengthen by coincident

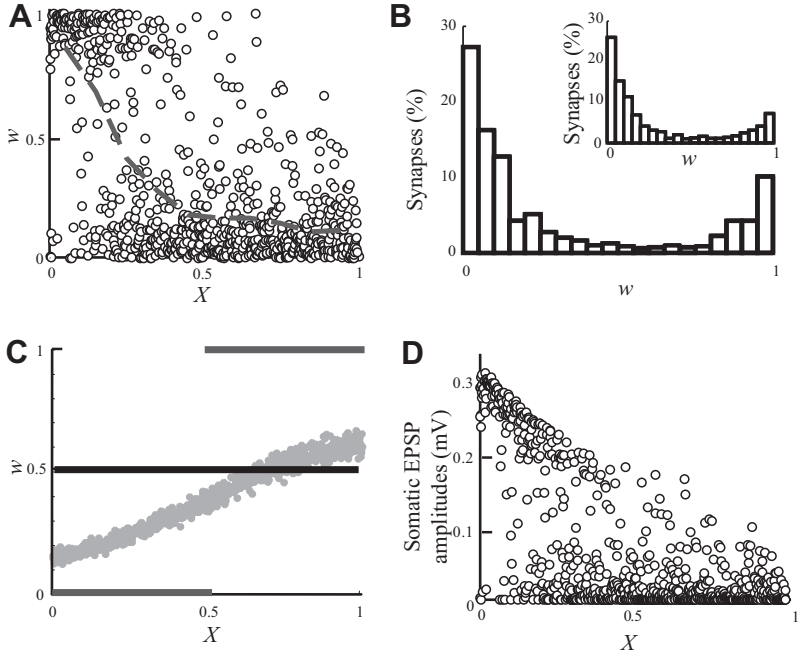

FIG. 1. "The problem" with spike-timing–dependent plasticity (STDP) in dendrites. Following STDP, the strength of distal synapses diminishes, whereas that of proximal synapses is enhanced. *A*: w as a function of electrotonic distance from the soma at steady state following STDP. The gray line depicts the average w (computed at 0.1 λ bins). Strong synapses ($w > 0.5$) almost vanish for $X > 0.5$. *B*: dendritic distribution of w values at steady state is bimodal. *Inset*: STDP in an isopotential compartment with the same membrane capacitance and conductance as in the dendritic model. *C*: 3 initial conditions for w were examined: w was set initially to 0.5 for all synapses (solid black line); w was arranged such that all synapses had the same efficacy at the soma (gray dots, see METHODS); $w = 0$ for synapses at $0 \leq X < 0.5$ and $w = 1$ for $0.5 \leq X \leq 1$ (gray lines). The steady-state weight distribution is identical for these different initial conditions and is shown in *A*. *D*: somatic excitatory postsynaptic potential (EPSP) amplitudes as a function of distance from the soma in steady state.

activity with the output. This way, proximal synapses may gain enough weight and regain their higher efficacy. After sufficient time, proximal synapses will win the competition over the distal synapses, albeit their initial ineffectiveness.

For comparison, we applied the linear STDP rule to an isopotential compartment with passive properties that are identical to the properties of the cylindrical cable. In this case, all the synapses have equal chances to be either weak or strong (Fig. 1*B*, *inset*) and the bimodal nature of the distribution also emerges (see Song et al. 2000). The somatic EPSP amplitudes following STDP at steady state against the distance of the synapses from the soma is depicted in Fig. 1*D*. The reduced weight of the distal synapses results from the filtering effect of the dendritic cable and the weakening of these synapses caused by STDP.

Location-independent scaling of synaptic weights does not "save" distal synapses

In an attempt to restore the balance in w, which is lost after STDP, we up-scaled the initial synaptic weights along the dendritic cylinder such that their efficacies were initially equal at (and thus independent of their distance from) the soma (Fig. 1*C*, gray dots, see METHODS). When the synaptic efficacies are equalized, an EPSP from distal synapses has the same probability as that of a proximal synapses to trigger a spike at the soma. In this case, on the face of it, STDP will not favor the proximal synapses over the distal synapses. However, imbalance in steady state persisted. Indeed, given that the cell is able to fire initially, the final distribution of synaptic weights was essentially independent of their initial distribution, similar to what was found in the isopotential case (Song et al. 2000). Thus up-scaling the synaptic conductance (their w value) of distal synapses will not rescue these synapses from dying out following STDP.

Dependence of β on the dendritic cable length and branching order

To capture the relation between the dendritic cable length and STDP, we varied the cable length, L, while keeping all other specific electrical parameters constant. Whereas in the short dendrite ($L = 0.4$; Fig. 2*A*), there are still some strong distal synapses following STDP, in the longer dendrite ($L = 1.8$; Fig. 2*C*), there are none. This increase in the weakening of distal synapses with L can be seen by comparing the steepness of the average w value in Fig. 2, *A–C* (heavy dashed line). This effect is summarized using β in Fig. 2*D*, for the three L values and for a range of mean synaptic weights, W, in each case (see METHODS). As L increases, the corresponding curve for β lies successively below one another, indicating that the degree on nonuniformity (or imbalance) in synaptic weight increases with increasing L.

To show that these results are caused by the increase in the dendritic cable length rather than by the increase in the number of synapses when L increases, we further examined the following two conditions (data not shown): *1*) the number of synapses remains constant while the dendritic length is varied, and *2*) the number of synapses is varied while keeping the length of the dendrite constant. β was reduced for condition *1*) but remained identical for all cases in condition *2*).

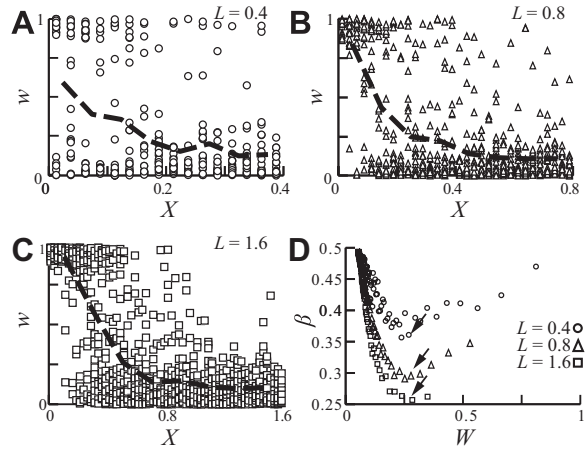

FIG. 2. The balance of the synaptic weight distribution is reduced for electrotonically longer dendrites. *A–C*: synapses were uniformly distributed over the cylindrical dendrite with $L = 0.4$ (*A*), $L = 0.8$ (*B*), and $L = 1.6$ (*C*). Synaptic weights at steady state are plotted against distance from the soma; heavy dashed line depicts the average synaptic weight, computed per 0.1 λ bins. Note the steeper decline of the average weight as L increases. Input rate is 13, 8, and 5 Hz for *A*, *B*, and *C*, respectively. *D*: β as a function of the mean synaptic weight, W. Each dot results from a different simulation, with a distinct input firing rate (4–60 Hz) resulting in different mean synaptic weight following STDP (see METHODS). As L increases, the curves reside one below the other (and in particular the minimum value of β decreases, arrows), implying that "the problem" becomes more severe when L increases.

We next examined in Fig. 3 the effect of the order of dendritic branching on the distribution of w at steady state following STDP. To isolate the effect of the branching on STDP, we used a set of idealized dendritic trees with an increasing order of branching, from zeroth-order (a cylinder) to third-order branching; all trees are equivalent to a single cylinder with $L = 1$ (see METHODS). In Fig. 3*A*, trees of zeroth and third order are shown in their physical scale and relative branch diameters (without the cell body). We first examined the case in which synaptic density per unit area was fixed, and synapses were distributed over the whole modeled trees. As expected from Rall (1959) because all trees are equivalent to the single cylinder, β is identical in all cases (Fig. 3*B*).

We further examined the case in which the synaptic density per unit λ was fixed. In this case, the density of synapses per unit area was greater for the higher order branching, and thus synaptic saturation was enhanced at these distal sites. This led to a decrease in the effectiveness of distal synapses compared with a corresponding model with uniform synaptic density per unit area. Figure 3*C* shows a small decrease in the minimal value of β (arrow) when the branching order increases. Because the higher density in the distal thinner branches results in marked synaptic saturation (loss of synaptic charge), the relatively small effect on β was surprising. Additional simulations with increased synaptic density at the distal dendritic regions (Elston and DeFelipe 2002; Marin-Padilla 1967) led to similar results of essentially small decreases in β (data not shown). This is explained by the reduced synaptic conductance (the weakening of synapses) at distal sites at steady state following STDP; consequently, synaptic saturation was less marked than that for the initial conditions. The proximal synapses eventually dominate the spike generation at the soma in both the unbranched tree and the branched tree.

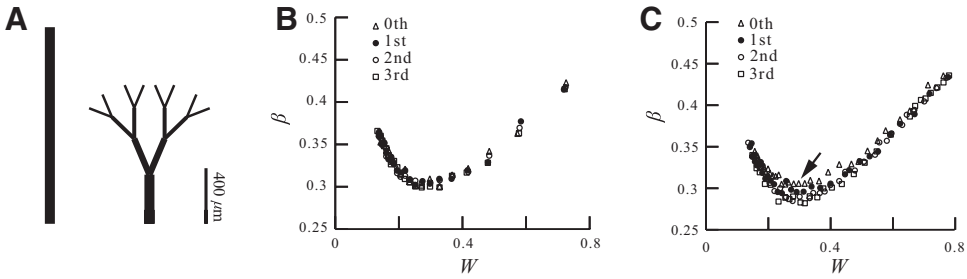

FIG. 3. STDP in branching dendrites. Idealized dendritic trees with a varying order of branching were modeled, all are electrically equivalent to a single cylinder with $L = 1$. *A*: 0th order (*left*) and 3rd order (*right*) branching. In all cases the trunk diameter is 4 μm; the 3rd-order branch diameter is 1 μm. *B*: β for 0th- to 3rd-order branching as a function of the average synaptic weigh value, *W*. Density of the synapses is uniform per unit area ($0.054/\mu m^2$). *C*: as in *B* but the density of the synapses is uniform per unit λ (600 synapses/λ). Only a slight decrease in the minimal β (black arrow) is observed in trees with higher branching orders.

STDP in reconstructed dendritic trees

We showed that increase in dendritic cable length rather than the degree of branching tends to weaken distal synapses. In Fig. 4, we examine these findings in reconstructed dendritic trees where STDP has been experimentally shown; L4 spiny stellate cell (Egger et al. 1999), L5 pyramid (Markram et al. 1997; Sjöström et al. 2001), and L2/3 pyramid (Feldman 2000; Froemke and Dan 2002). Because we are interested here in the effect of dendritic morphology per se on the outcome of STDP, we assumed that these dendrites have identical passive properties (see METHODS) and the same density of synapses per unit area ($0.02/\mu m^2$). To compare between the models' distribution of the weights, we selected results from simulations where the mean synaptic weight (*W*) at steady state was equal in all of the model neurons. In Fig. 4, the value of *w* at steady state for the corresponding neurons is shown as a function of the electrotonic distance of the synapses from the soma.

Although the "problem" exists in all the reconstructed dendrites, it is more severe in electrotonically long dendrites. Figure 4*D* summarizes how strong synapses ($w > 0.5$) are divided between the proximal ($X/L > 0.5$) and distal ($X/L < 0.5$) regions for the modeled neurons. L5 dendrites that extends up to $\sim 2\ \lambda$ have $<5\%$ of the strong synapses in the distal region, whereas the electrically compact L4 spiny stellate cell ($\sim 0.4\ \lambda$ long) is more balanced, so that $\sim 40\%$ of its strong synapses are in the distal region. The L2/3 pyramid ($\sim 0.6\ \lambda$ long) is somewhere in between with $\sim 25\%$ of its strong synapses in the distal region.

Rescuing distal synapses with a multiplicative STDP learning rule

In Fig. 5, multiplicative STDP (see METHODS) was applied in the cylindrical neuron model, and the distribution of synaptic weights in steady state was examined for various values of μ, starting from $\mu = 0$ (additive rule) and up to $\mu = 1$ (fully multiplicative). The competition between synapses is significantly reduced when μ is increased (Gütig et al. 2003). This is followed by the "compression" of the synaptic weights to a midrange values ($w = 0.5$). As can be seen in Fig. 5*A*, for strong multiplicative cases ($\mu = 1$), the weight of distal and proximal synapses tends to be equal. However, in this extreme case, all synaptic weights are "stuck" near the value of 0.5.

In Fig. 5*B*, with a very small $\mu = 0.5^4$ (close to fully additive case), distal synapses were partially rescued from completely dying out (as was the case for the additive STDP; Fig. 2), and the synaptic weights were distributed over an acceptable range of values. Nevertheless, in this case, STDP is still biased in favor of the proximal synapses. A summary for the distribution of β values for different values of μ is depicted in Fig. 5*C*. The weights distribution becomes significantly more balanced (closer to 0.5) when μ approaches 1.

A combination of homeostatic synaptic plasticity and a "mixed" STDP rule that was proposed by van Rossum et al. (2000) results in a unimodal distribution of EPSP amplitudes (unlike the bimodal distribution in the additive STDP case). Although we did not reproduce their model, we expect that using this model for STDP will also help in rescuing distal synapses similarly to the multiplicative model as in Fig. 5.

We have shown in this section that a weak multiplicative STDP rule may partially rescue the distal synapses from dying out. A strong multiplicative STDP rule, however, while improving the uniformity of synaptic strength over the dendritic tree, results in "gluing" all synaptic weights near the midrange value of 0.5. This is undesirable because, under this condition, synapses are effectively not plastic anymore.

Rescuing distal synapses with a spatial gradient of g_{max}

We have shown that an initial location-independent distribution of synaptic weights does not save distal synapses from dying out following STDP (Fig. 1*C*, dotted line). We therefore propose an alternative possibility whereby a certain form of meta-plasticity, as suggested by Abraham and Bear (1996), could be used for saving distal synapses from dying out following STDP (see also Gidon and Segev 2005; Rumsey and Abbott 2006). Namely, we scaled the maximal strength (g_{max}) that the synapse may potentially undergo instead of scaling the actual initial strength, g_{peak}, of the synaptic conductance. In other words, we up-scaled g_{max} as a function of distance from the soma so that all synapses have identical efficacies at the soma (synaptic democracy) while keeping $w = 0.5$ for all synapses (see METHODS and Fig. 6*A*). Now, with such scaling of g_{max}, the distribution of *w* at steady state following STDP is spatially much more balanced (Fig. 6*A*) compared with the case of uniform g_{max} distribution (Fig. 6*B*). The tendency toward a more balanced weight distribution is also observed in the multiplicative learning rule (data not shown).

How robust is the balance of synaptic weight distribution (synaptic democracy) that resulted from scaling of g_{max} under varying input frequencies? In Fig. 6*A*, g_{max} was scaled such that synaptic

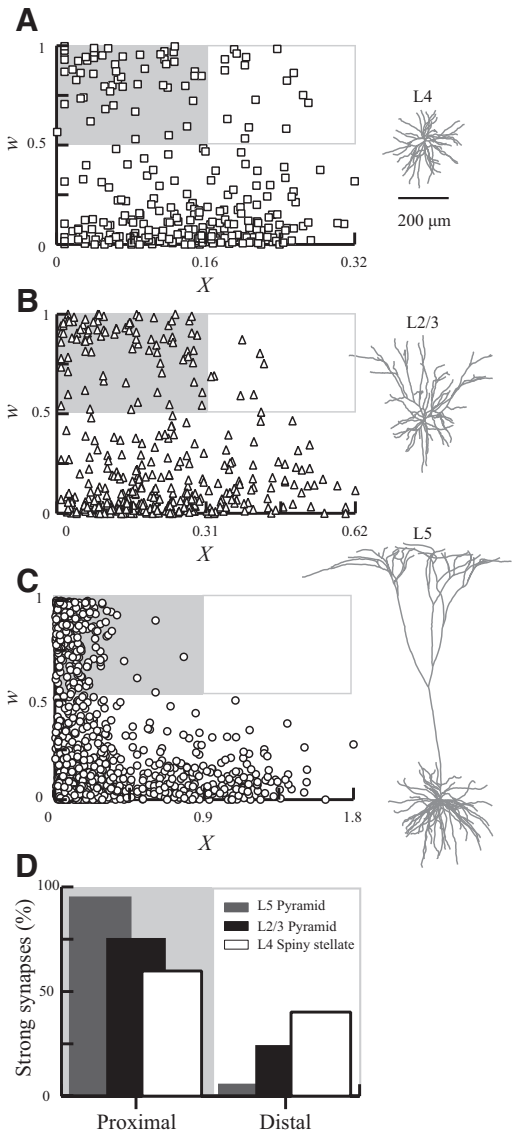

FIG. 4. STDP in modeled reconstructed neurons. The unbalanced weight distribution at steady state following STDP is shown in L4 (*A*) cortical spiny stellate cell, in L2/3 pyramid neuron (*B*), and in L5 pyramid neuron (*C*). Presynaptic rate in each tree was chosen so that *W* was similar in all trees at steady state (0.30, 0.29, and 0.29 for *A*, *B,* and *C,* respectively). The proximal region with strong synapses ($X/L < 0.5$; $w > 0.5$) is marked by gray rectangle and the distal region with strong synapses ($X/L > 0.5$; $w > 0.5$) is marked with white rectangle. *D*: percentage of strong ($w > 0.5$) proximal or distal synapses out of the total strong synapses averaged over multiple simulation runs ($n = 30$) of each of the neuron models *A–C* (background as in *A–C*). The percentage of strong synapses in the proximal region is 95, 75, and 60% for L5, L2/3, and L4 spiny stellate, respectively.

democracy is achieved with a mean input rate of 10 Hz. Changing the input rate is expected to change the effective length constant, λ_{eff}, (see METHODS) and thus the cable distance of any given synapse from the soma. This in turn may destroy the spatial balance (democracy) of synaptic efficacy. To examine this, we plotted in Fig. 6*C* the value β as a function of *W* (ranging the input frequency from 4 to 51 Hz). The resulting flat curve (triangles) shows that, although g_{max} was adjusted only for an input rate of 10 Hz, the spatial balance of synaptic efficacy is essentially sustained for all input frequencies (the minimal value of β is ~0.45). In contrast, β is reduces to 0.27 when g_{max} is uniform (circles).

To better understand this unexpected result, we computed the value of λ_{eff} as a function of *W* (and thus of the input frequency). Before STDP was applied, λ_{eff} was reduced by a factor of 2.6 when the input frequency ranged from 4 to 51 Hz. Namely, the electrotonic length of the cable was increased by 2.6-fold (Fig. 6*D*, dark dots). This implies that the distance, in λ units, of any given synapse from the soma is stretched by almost a factor of 3 as a consequence of the increase in input frequency (from 4 to 51 Hz). However, when the initial input rate is high, STDP causes a decrease in the mean synaptic weight (and in the number of strong synapses, Song et al. 2000). The reduction in the total synaptic conductance counterbalances the high input rates and, thus λ_{eff} remains rather constant albeit the change in input frequency (Fig. 6*D*, ○). The consequence is that the spatial distribution of synaptic weights following the scaling of g_{max} remains balanced (democratic) even with a change in input frequency.

DISCUSSION

In this computational exploration of the functional consequences of STDP in dendrites, we highlighted the existence of an inherent problem in this mechanism. Namely, as the STDP process proceeds, distal dendritic synapses will become progressively "dominated" by the proximal synapses. We assumed in this work that the STDP rule is uniform over the whole dendritic surface; yet recent results showed that the STDP rule itself may vary in the same dendrite such that long-term depression (LTD) is more prominent in distal regions, whereas long-term potentiation (LTP) is more prominent in proximal regions (Froemke et al. 2005; Letzkus et al. 2006; Sjöström and Häusser 2006). In the light of these findings, the problem with STDP that we discussed in this work seems to be even more acute because rather than compensate for their decreased efficacy, the location-dependent modifications in the STDP rule itself seem to act against distal synapses.

We systematically studied the dendritic determinants of this "problem" with STDP in dendrites; namely, the dendritic cable length, branching order, and spatial distribution of synapses on the dendritic tree. The electrotonic length of the dendrite has the most prominent effect; distal synapses on long dendrites become completely ineffective following STDP. This holds regardless of both changing the synaptic distributions and of the dendritic branching pattern.

We next systematically examined several ways to balance the distribution of synaptic weights in the dendritic tree. We explored the possibility that the STDP rule is not purely additive, but rather includes a multiplicative component (denoted by μ; see Fig. 5 and *Eqs. 3* and *4*; see Gütig et al. 2003). We showed that increasing the value of μ could rescue distal synapses. However, the multiplicative STDP rule balances the weights distribution ($\beta = 0.5$) by bracketing the range of synaptic strength to a mid-range value (of 0.5), thus restricting the dynamical range of synaptic efficacy.

We showed that imposing initial "location independence" of the somatic EPSPs cannot rescue distal synapses from dying out following STDP. Indeed, when g_{max} is spatially uniform, distal synapses are a priori disadvantageous compared with proximal synapses because they are less effective at the soma even when they become maximally strengthened and gain the value of g_{max}. Even if initially g_{peak} is zero at proximal sites,

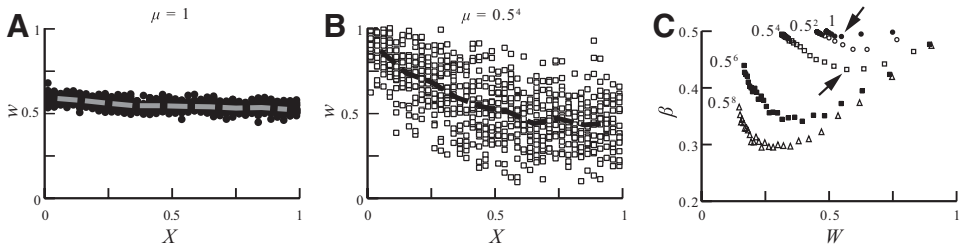

FIG. 5. Rescuing distal synapses with a multiplicative STDP rule. *A:* synaptic weight as a function of distance from soma for the strong multiplicative case ($\mu = 1$). Weights of distal and proximal synapses are "stuck" around $w = 0.5$ with a small advantage of proximal synapses (averaged weight per 0.1 λ is depicted by the dashed line). *B*: weak multiplicative case ($\mu = 0.5^4$). Larger variance in w coincides with an increase in the difference between proximal and distal synapses, yet distal synapses do not completely die out. *C*: β a function of W with various values of μ (marked next to graphs). As μ is reduced (more linear STDP rule), the uniformity of synaptic weight over the dendritic tree is reduced (β decreases). Marked with arrows are β values depicted in *A* and *B*. A cylindrical dendritic model with $L = 1$ is used.

proximal synapses eventually win over distal synapses (Fig. 1). Thus it is the "ceiling" effect (the value of g_{max}) that matters for this "proximal versus distal competition" at steady state, rather than the value of g_{peak} per se at any given location.

In contrast, we showed that if g_{max} is distributed spatially so that the somatic EPSP is "location independent" (Gidon and Segev 2005; Rumsey and Abbott 2006), the spatial distribution of synaptic weights following STDP is uniform at steady state (Fig. 6*C*). Surprisingly, we found that the uniform weights distribution caused by g_{max} scaling is very robust to changes in input rate and/or number of synapses impinging on the dendrites (Fig. 6*D*); this makes g_{max} scaling a favorable mechanism for maintaining democracy among the dendritic synapses. Furthermore, combining this mechanism with the multiplicative STDP yielded the most balanced dendritic weights distribution (data not shown). Indeed, the experimental findings of an increase in AMPA current (Andrasfalvy and Magee 2001; Magee and Cook 2000), of more perforated synapses (Nicholson et al. 2006; Nimchinsky et al. 2002) and of larger spine head size (Megias et al. 2001; Konur et al. 2003) in distal dendrites could support the possibility that g_{max} is indeed up-scaled with distance.

Experimental validation of g_{max} scaling

The saturation of LTP was studied in the context of metaplasticity (Abraham and Bear 1996) primarily to assess their post-LTP responsiveness. In our model, saturation of LTP is, by definition, the point at which g_{peak} is equal to g_{max} (i.e., $w = 1$). We suggest to experimentally measure the distribution of synaptic conductances (or of local amplitude of the synaptic current) over the dendritic surface after saturation of the synaptic conductances following STDP protocol and thus to uncover the value of g_{max} at each dendritic location. Cells that exhibit a somato-dendritic gradient of g_{peak} (as in CA1 neurons; see Andrasfalvy and Magee 2001) both before and after STDP saturation would support the hypothesis that g_{max} is indeed scaled up with distance. This hypothesis will be rejected if the synaptic conductance change following STDP saturation is similar for all synapses independent of their distance from the soma.

Other possible mechanisms for "saving" distal synapses

A variety of homeostatic synaptic plasticity (HSP) mechanisms (Lissin et al. 1998; O'Brien et al. 1998; Turrigiano et al. 1998) may coexist in dendrites together with STDP and could contribute to synaptic democracy (Earnshaw and Bressloff 2008). Because the time constant of HSP is typically much longer (hours) than that of STDP, if both mechanisms operate on the same biophysical parameter (e.g., the density of APMA receptors), we found that HSP does not counterbalance STDP (simulation results not shown). However, if HSP modulates synaptic efficacy through a different biophysical parameter (e.g., g_{max}) than does STDP, HSP could contribute to dendritic democracy.

Dendrites are known have active (nonlinear) voltage-dependent conductances. *N*-methyl-D-aspartate (NMDA) spikes (Schiller et al. 2000), dendritic calcium and sodium spikes (Araya et al. 2007; Kampa et al. 2007; Yuste et al. 1994), and other active currents like the I_h (Magee 1999; Robinson and Siegelbaum 2003) are engaged in the process of synaptic integration (Magee 2000) and computation (London and Häusser 2005) in dendrites. A special case for dendritic nonlinearity is the case of action potential generation in the spine head membrane (Araya et al. 2007). In an initial set of simulations that approx-

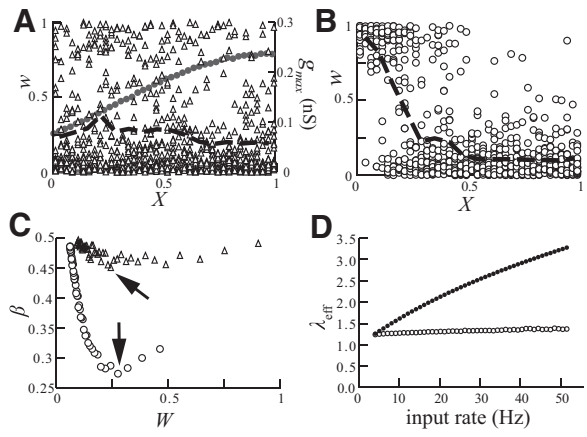

FIG. 6. Saving distal synapses from dying out via up-scaling of g_{max} with distance from soma. *A:* distribution of w (triangles) at steady state is balanced (averaged weight per 0.1 λ is depicted by the black dashed line) following up-scaling of g_{max} (gray line) for input rate of 10 Hz. *B*: weight distribution for the case where g_{max} is spatially uniform (=0.3 nS). *C*: summary of β value for the case where g_{max} is up-scaled (triangles) and uniform (circles). Note that, although synaptic efficacy was equalized for 10 Hz, the weights distribution was balanced (β near 0.5, triangles) for all W values (input rates 4–51 Hz). Arrows indicate β values for the cases depicted in *A* and *B*. *D*: the effective space constant, λ_{eff}, is preserved by STDP. Before STDP, λ_{eff} is increased by 2.6-fold with increased input rate from 4 to 51 Hz (dots). However, at steady state following STDP, λ_{eff} is essentially independent of the input frequency (open circles).

imate this case whereby excitable current boosts spiny synapses, we found that, if the threshold for nonlinearly boosting distal synaptic efficacy is low (namely, small *w* value may reach this threshold), indeed distal synapses may win over proximal synapses following STDP (data not shown). A complete study on the effect of dendritic nonlinearity interacting with STDP is underway.

These mechanisms are able to effectively augment the efficacies of synapses, in particularly that of the distal synapses (Bernander et al. 1994; De Schutter and Bower 1994) so that the efficacy of synapses is not dominated only by passive properties of the dendritic cable. In fact, calcium spikes were shown to have an important role in determining the efficacy of the STDP induction process (Kampa et al. 2006). Perhaps these dendritic mechanisms could shift the balance of the synaptic weights to distal dendritic regions? Indeed, this study should be viewed as providing the fundamental solutions for the "problem" with STDP in dendrites in the passive case. It provides the basis—or skeleton—on which more complex nonlinear dendritic currents should be added and their affects on STDP in dendrites better understood (Rumsey and Abbott 2006; Sjöström et al. 2008).

GRANTS

This work was supported by a grant from the Edmond J. Safra Foundation (Learning and Memory), by the National Institutes of Health, and by the Israeli Science Foundation.

REFERENCES

Abbott LF, Nelson SB. Synaptic plasticity: taming the beast. *Nat Neurosci* 3: 1178–1183, 2000.

Abraham W, Bear M. Metaplasticity: the plasticity of synaptic plasticity. *Trends Neurosci* 19: 126–130, 1996.

Andrasfalvy BK, Magee JC. Distance-dependent increase in AMPA receptor number in the dendrites of adult hippocampal CA1 pyramidal neurons. *J Neurosci* 21: 9151–9159, 2001.

Araya R, Nikolenko V, Eisenthal K, Yuste R. Sodium channels amplify spine potentials. *Proc Natl Acad Sci USA* 104: 12347–12352, 2007.

Ascoli G. Mobilizing the base of neuroscience data: the case of neuronal morphologies. *Nat Rev Neurosci* 7: 318–324, 2006.

Bell CC, Han VZ, Sugawara Y, Grant K. Synaptic plasticity in a cerebellum-like structure depends on temporal order. *Nature* 387: 278–281, 1997.

Bernander O, Koch C, Douglas RJ. Amplification and linearization of distal synaptic input to cortical pyramidal cells. *J Neurophysiol* 72: 2743–2753, 1994.

Bi GQ, Poo MM. Synaptic modifications in cultured hippocampal neurons: dependence on spike timing, synaptic strength, and postsynaptic cell type. *J Neurosci* 18: 10464–10472, 1998.

Bi GQ, Wang HX. Temporal asymmetry in spike timing-dependent synaptic plasticity. *Physiol Behav* 77: 551–555, 2002.

Dan Y, Poo MM. Spike timing-dependent plasticity: from synapse to perception. *Physiol Rev* 86: 1033–1048, 2006.

De Schutter E, Bower JM. Simulated responses of cerebellar Purkinje cells are independent of the dendritic location of granule cell synaptic inputs. *Proc Natl Acad Sci USA* 91: 4736–4740, 1994.

Debanne D, Gähwiler BH, Thompson SM. Long-term synaptic plasticity between pairs of individual CA3 pyramidal cells in rat hippocampal slice cultures. *J Physiol* 507: 237–247, 1998.

Douglas RJ, Martin KA, Whitteridge D. An intracellular analysis of the visual responses of neurones in cat visual cortex. *J Physiol* 440: 659–696, 1991.

Earnshaw BA, Bressloff PC. Modeling the role of lateral membrane diffusion in AMPA receptor trafficking along a spiny dendrite. *J Comput Neurosci* 25: 366–389, 2008.

Egger V, Feldmeyer D, Sakmann B. Coincidence detection and changes of synaptic efficacy in spiny stellate neurons in rat barrel cortex. *Nat Neurosci* 2: 1098–1105, 1999.

Elston GN, DeFelipe J. Spine distribution in cortical pyramidal cells: a common organizational principle across species. *Prog Brain Res* 136: 109–133, 2002.

Feldman DE. Timing-based LTP and LTD at vertical inputs to layer II/III pyramidal cells in rat barrel cortex. *Neuron* 27: 45–56, 2000.

Froemke R, Poo MM, Dan Y. Spike-timing-dependent synaptic plasticity depends on dendritic location. *Nature* 434: 221–225, 2005.

Froemke RC, Dan Y. Spike-timing-dependent synaptic modification induced by natural spike trains. *Nature* 416: 433–438, 2002.

Froemke RC, Tsay IA, Raad M, Long JD, Dan Y. Contribution of individual spikes in burst-induced long-term synaptic modification. *J Neurophysiol* 95: 1620–1629, 2006.

Gidon A, Segev I. Conducting STDP in dendrites. Abstracts of the 13th Annual Meeting of Israel Society for Neuroscience. *Neural Plasticity* 12: 1–68, 2005.

Goldberg J, Holthoff K, Yuste R. The problem with Hebb and local spikes. *Trends Neurosci* 25: 433–435, 2002.

Gütig R, Aharonov R, Rotter S, Sompolinsky H. Learning input correlations through nonlinear temporally asymmetric Hebbian plasticity. *J Neurosci* 23: 3697–3714, 2003.

Hebb D. *The Organization of Behaviour.* New York: Wiley, 1949.

Hines ML, Carnevale NT. The NEURON simulation environment. *Neural Comput* 9: 1179–1209, 1997.

Iannella N, Tanaka S. Synaptic efficacy cluster formation across the dendrite via STDP. *Neurosci Lett* 403: 24–29, 2006.

Kampa BM, Letzkus JJ, Stuart GJ. Requirement of dendritic calcium spikes for induction of spike-timing-dependent synaptic plasticity. *J Physiol* 574: 283–290, 2006.

Kampa BM, Letzkus JJ, Stuart GJ. Dendritic mechanisms controlling spike-timing-dependent synaptic plasticity. *Trends Neurosci* 30: 456–463, 2007.

Kempter R, Leibold C, Wagner H, van Hemmen JL. Formation of temporal-feature maps by axonal propagation of synaptic learning. *Proc Natl Acad Sci USA* 98: 4166–4171, 2001.

Kistler WM, van Hemmen JL. Modeling synaptic plasticity in conjunction with the timing of pre- and postsynaptic action potentials. *Neural Comput* 12: 385–405, 2000.

Konur S, Rabinowitz D, Fenstermaker VL, Yuste R. Systematic regulation of spine sizes and densities in pyramidal neurons. *J Neurobiol* 56: 95–112, 2003.

Letzkus JJ, Kampa BM, Stuart GJ. Learning rules for spike timing-dependent plasticity depend on dendritic synapse location. *J Neurosci* 26: 10420–10429, 2006.

Lissin DV, Gomperts SN, Carroll RC, Christine CW, Kalman D, Kitamura M, Hardy S, Nicoll RA, Malenka RC, von Zastrow M. Activity differentially regulates the surface expression of synaptic AMPA and NMDA glutamate receptors. *Proc Natl Acad Sci USA* 95: 7097–7102, 1998.

London M, Häusser M. Dendritic computation. *Annu Rev Neurosci* 28: 503–532, 2005.

Magee JC. Dendritic Ih normalizes temporal summation in hippocampal CA1 neurons. *Nat Neurosci* 2: 848, 1999.

Magee JC. Dendritic integration of excitatory synaptic input. *Nat Rev Neurosci* 1: 181–190, 2000.

Magee JC, Cook EP. Somatic EPSP amplitude is independent of synapse location in hippocampal pyramidal neurons. *Nat Neurosci* 3: 895–903, 2000.

Marin-Padilla M. Number and distribution of the apical dendritic spines of the layer V pyramidal cells in man. *J Comp Neurol* 131: 475–490, 1967.

Markram H, Lübke J, Frotscher M, Sakmann B. Regulation of synaptic efficacy by coincidence of postsynaptic APs and EPSPs. *Science* 275: 213–215, 1997.

Meffin H, Besson J, Burkitt AN, Grayden DB. Learning the structure of correlated synaptic subgroups using stable and competitive spike-timing-dependent plasticity. *Phys Rev E Stat Nonlin Soft Matter Phys* 73: 041911, 2006.

Megias M, Emri Z, Freund TF, Gulyas AI. Total number and distribution of inhibitory and excitatory synapses on hippocampal CA1 pyramidal cells. *Neuroscience* 102: 527–540, 2001.

Nicholson DA, Trana R, Katz Y, Kath WL, Spruston N, Geinisman Y. Distance-dependent differences in synapse number and AMPA receptor expression in hippocampal CA1 pyramidal neurons. *Neuron* 50: 431–442, 2006.

Nimchinsky EA, Sabatini BL, Svoboda K. Structure and function of dendritic spines. *Annu Rev Physiol* 64: 313–353, 2002.

O'Brien RJ, Kamboj S, Ehlers MD, Rosen KR, Fischbach GD, Huganir RL. Activity-dependent modulation of synaptic AMPA receptor accumulation. *Neuron* 21: 1067–1078, 1998.

Rabinowitch I, Segev I. The interplay between homeostatic synaptic plasticity and functional dendritic compartments. *J Neurophysiol* 96: 276–283, 2006.

Rall W. Branching dendritic trees and motoneuron membrane resistivity. *Exp Neurol* 1: 491–527, 1959.

Rall W. Distinguishing theoretical synaptic potentials computed for different soma-dendritic distributions of synaptic input. *J Neurophysiol* 30: 1138–1168, 1967.

Rao RPN, Sejnowski TJ. Spike-timing-dependent Hebbian plasticity as temporal difference learning. *Neural Comput* 13: 2221–2237, 2001.

Roberts PD. Modeling inhibitory plasticity in the electrosensory system of mormyrid electric fish. *J Neurophysiol* 84: 2035–2047, 2000.

Roberts PD, Bell CC. Computational consequences of temporally asymmetric learning rules. II. Sensory image cancellation. *J Comput Neurosci* 9: 67–83, 2000.

Robinson RB, Siegelbaum SA. Hyperpolarization-activated cation currents: from molecules to physiological function. *Annu Rev Physiol* 65: 453–480, 2003.

Roth A, London M. Rebuilding dendritic democracy. Focus on "equalization of synaptic efficacy by activity- and timing-dependent synaptic plasticity". *J Neurophysiol* 91: 1941–1942, 2004.

Rubin J. Steady states in an iterative model for multiplicative spike-timing-dependent plasticity. *Network* 12: 131–140, 2001.

Rubin J, Lee DD, Sompolinsky H. Equilibrium properties of temporally asymmetric Hebbian plasticity. *Phys Rev Lett* 86: 364–367, 2001.

Rumsey CC, Abbott LF. Equalization of synaptic efficacy by activity- and timing-dependent synaptic plasticity. *J Neurophysiol* 91: 2273–2280, 2004.

Rumsey CC, Abbott LF. Synaptic democracy in active dendrites. *J Neurophysiol* 96: 2307–2318, 2006.

Saudargiene A, Porr B, Wörgötter F. Local learning rules: predicted influence of dendritic location on synaptic modification in spike-timing-dependent plasticity. *Biol Cybern* 92: 128–138, 2005a.

Saudargiene A, Porr B, Wörgötter F. Synaptic modifications depend on synapse location and activity: a biophysical model of STDP. *Biosystems* 79: 3–10, 2005b.

Schiller J, Major G, Koester H, Schiller Y. NMDA spikes in basal dendrites of cortical pyramidal neurons. *Nature* 404: 285–289, 2000.

Shouval HZ, Bear MF, Cooper LN. A unified model of NMDA receptor-dependent bidirectional synaptic plasticity. *Proc Natl Acad Sci USA* 99: 10831–10836, 2002.

Sjöström PJ, Häusser M. A cooperative switch determines the sign of synaptic plasticity in distal dendrites of neocortical pyramidal neurons. *Neuron* 51: 227–238, 2006.

Sjöström PJ, Rancz EA, Roth A, Häusser M. Dendritic excitability and synaptic plasticity. *Physiol Rev* 88: 769–840, 2008.

Sjöström PJ, Turrigiano G, Nelson S. Rate, timing, and cooperativity jointly determine cortical synaptic plasticity. *Neuron* 32: 1149–1164, 2001.

Song S, Abbott LF. Cortical development and remapping through spike timing-dependent plasticity. *Neuron* 32: 339–350, 2001.

Song S, Miller KD, Abbott LF. Competitive Hebbian learning through spike-timing-dependent synaptic plasticity. *Nat Neurosci* 3: 919–926, 2000.

Traub RD, Wong RK, Miles R, Michelson H. A model of a CA3 hippocampal pyramidal neuron incorporating voltage-clamp data on intrinsic conductances. *J Neurophysiol* 66: 635–650, 1991.

Turrigiano GG, Leslie KR, Desai NS, Rutherford LC, Nelson SB. Activity-dependent scaling of quantal amplitude in neocortical neurons. *Nature* 391: 892–896, 1998.

Urakubo H, Aihara T, Kuroda S, Watanabe M, Kondo S. Spatial localization of synapses required for supralinear summation of action potentials and EPSPs. *J Comput Neurosci* 16: 251–256, 2004.

van Rossum MC, Bi GQ, Turrigiano GG. Stable Hebbian learning from spike timing-dependent plasticity. *J Neurosci* 20: 8812–8821, 2000.

Vetter P, Roth A, Häusser M. Propagation of action potentials in dendrites depends on dendritic morphology. *J Neurophysiol* 85: 926–937, 2001.

Williams A, Roberts PD, Leen TK. Stability of negative-image equilibria in spike-timing-dependent plasticity. *Phys Rev E Stat Nonlin Soft Matter Phys* 68: 021923, 2003.

Yuste R, Gutnick M, Saar D, Delaney K, Tank D. Ca^{2+} accumulations in dendrites of neocortical pyramidal neurons: an apical band and evidence for two functional compartments. *Neuron* 13: 23–43, 1994.

Zhang LI, Tao HW, Holt CE, Harris WA, Poo MM. A critical window for cooperation and competition among developing retinotectal synapses. *Nature* 395: 37–44, 1998.